Compressive strength and microstructure of alkali-activated blast furnace slag/sewage sludge ash (GGBS/SSA) blends cured at room temperature

M.M. Tashima[1*], L. Reig[2], M.A. Santini Jr.[1], J.C.B Moraes[1], J.L. Akasaki[1], J. Payá[3], M.V. Borrachero[3], L. Soriano[3]

[1] UNESP – Univ Estadual Paulista, campus de Ilha Solteira, SP- Brazil. MAC/UNESP – grupo de pesquisa em Materiais Alternativos de Construção.

[2] EMC, Universitat Jaume I, Castelló de la Plana - Spain.

[3] ICITECH - Instituto de Ciencia y Tecnología del Hormigón. GIQUIMA group, Universitat Politècnica de València.

* Corresponding author: maumitta@hotmail.com; mmtashima@dec.feis.unesp.br

Abstract

In the present work, ground granulated blast furnace slag (GGBS) and sewage sludge ash (SSA) blends were assessed for the production of alkali-activated pastes and mortars. Percentages of SSA to substitute GGBS ranged from 0–30 wt.% and sodium concentrations of 6–10 mol.kg^{-1} were used for the activating solutions. Pastes and mortars were cured at 20 ℃ for up to 90 days. Raw materials were characterised by granulometric analysis, XRF, XRD, FTIR and SEM techniques. The replacement percentage of GGBS by SSA and the sodium hydroxide concentration of the alkaline activator were optimised to produce mortar with compressive strengths close to 30 MPa after 28 curing days at room temperature. Best results were obtained in samples blended with 20 wt.% SSA activated with 6 mol.kg^{-1} NaOH solutions which, according to the XRD, FTIR and microscopic results, contained higher amounts of (N,C)-A-S-H gel. The potential use of SSA for the development of alternative cementitious materials at room temperature has been demonstrated.

Keywords: Sewage Sludge Ash, Waste Management, Alkali-Activated Cement, Compressive Strength.

1. Introduction

Sewage sludge is a residue that results from the treatment of municipal wastewaters; it is generated in physical-chemical processes such as coagulation, flocculation and sedimentation. Reutilisation and stabilisation of sewage sludge results in a very interesting environmental solution, because it contains pathogens, parasites and toxic agents making it a hazardous material that cannot be disposed in any place [1]. It is estimated that approximately 0.15–0.22 million tons of dry sewage sludge are produced yearly in Brazil [2] while, according to Baeza-Brotons et al. [3], 1.07 million tons of dry sewage sludge is generated yearly in Spain. Similarly, more than 3 million tons of dry sewage sludge was generated in the Baltic Sea Region in 2010; this amount is expected to increase by 14.4% by 2020 [4].

Sewage sludge is commonly disposed in landfills, treated for fertiliser production, or dumped in rivers and oceans. According to the European Commission, approximately 65% of sewage sludge is used as fertiliser, 20% is deposited in controlled landfills, and 10% is incinerated. Incineration is used for reducing the volume of the waste and it is not widely utilised worldwide. Comparatively, according to the Spanish government [5], about 88% of sewage sludge is used as fertiliser, 8% landfilled and 4% is incinerated.

Data reported by Pedrosa et al. [2] indicates that in Brazil only 30% of the sewage collected is treated, leading to high amounts of sewage sludge being sent to landfill, creating serious environmental problems. Donatello and Cheeseman [6] explain that concerns regarding contaminants and heavy metals in sewage sludge have prompted health agencies to establish new regulations which limit the use of this waste material as fertiliser. In this sense, the incineration of sewage sludge is an environmentally friendly solution that not only reduces its volume, but can also be used to generate energy [4].

Sewage sludge ash (SSA) is produced during the combustion of dewatered sewage sludge using an incinerator. This ash is collected at the base of a combustion chamber (known as bottom ash) or in electrostatic precipitator systems (known as fly ash). Although the ash is mainly composed of SiO_2, Al_2O_3, Fe_2O_3, CaO, Na_2O, MgO, SO_3 and P_2O_5 [7], the specific composition varies depending on the origin of the wastewater and its treatment processes. Similarly, the particle size and characteristics of the ash highly depend on the incineration system [4]. According to Yusuf et al. [8], incineration of the sludge reduces its volume by 95%, while studies performed in the United Kingdom have concluded that the mass

of the sludge is reduced to 1% of the original and that the ash is sterile and inert [1]. Cheeseman and Virdi [1] explain that although this ash is not considered a hazardous waste, concerns about the high heavy metal contents have limited its use in agriculture or in landfill disposals.

SSA is generated continuously and in relatively large amounts in treatment plants. It is estimated that approximately 1.7 million tons of sewage sludge ash is produced worldwide annually [6] while, according to a review by Yusuf et al. [8], approximately 1.2 million tons of SSA is produced in the European Union and North America, and 0.5 million tons is produced in Japan. Baeza-Brotons et al. [3] estimate the amount of incinerated sludge will increase by 20–25% by 2020 in Spain.

The prospect of future increases in sewage sludge production coupled with the fact that the majority of the SSA is still being sent to landfill has prompted the scientific community to develop new techniques in order to reuse waste in the development of construction materials. In the construction industry, sustainable building practices employ techniques to reuse wastes as useful parts, or utilise them to produce new building elements. Both techniques benefit the environment: the reduction of industrial waste relieves landfills; natural raw materials are conserved; and energy consumtion is reduced during the production of the recycled products. Additional potential benefits of using SSA in construction materials include immobilising heavy metals in a developed matrix. Yusuf et al. [8] reported that the amount of heavy metals leached in ordinary Portland cement (OPC) mortars containing SSA was similar to that of reference mortars (only OPC). Additionally, Yang et al. [9] have previously analysed the durability of autoclaved bricks produced using SSA/OPC/FA/GGBS blends. Their conclusions suggest that the concentrations of heavy metals leached from the produced bricks were much lower than that established by Chinese government regulations.

Sewage sludge ashes have been successfully used to produce different types of building materials [4]: they have been used as a raw material for cement production; as a pozzolanic admixture in cementitious binders [10–11]; they have been used in the manufacture of building elements such as concrete blocks [3]; they can be used to produce lightweight recycled aggregates in the production of concrete [12–13]; or used as a partial substitute of soil or cement when stabilising road bases. According to Yusuf et al [8], SSA particles have an irregular shape and a porous structure; this creates a high water demand when they

are used in concrete mixtures, leading to a slight reduction of their workability and strength. Similar behaviour has been shown in studies by Monzó et al. [10–11] who observed a reduction in the workability of mortars with an increased SSA content. This is due to the behaviour attributed to the irregular shape and to the high water absorption of SSA particles. In these studies, authors have successfully proved the pozzolanic properties of SSA, allowing the use of SSA as a partial replacement for Portland cement. The replacement of 15–30 wt.% of OPC by SSA generally increases the compressive strength of mortars cured at 40 ºC for up to 28 days, mainly for short curing ages.

Alkali-activated (AA) binders are considered alternative binding materials. They are produced by a chemical reaction between an aluminosilicate-based mineral (precursor) and an alkaline reagent (activating solution). The aluminosilicate compounds of a given precursor are dissolved in a highly alkaline medium allowing the formation of a new binding gel. This gel contains tetrahedral SiO_4 and AlO_4 units which are randomly distributed in chains and 3D-networks. Alkali metal cations (typically Na^+ and/or K^+) balance the negative charges of the tetrahedral-linking network [14].

AA binders based on ground granulated blast furnace slag (GGBS) have been extensively reported on in the literature. These studies have demonstrated the good performance of these alternative binders in relation to both mechanical and durability properties [15]. According to Shi et al. [15], alkali-activated mortars based on slag can yield about 120 MPa in compression following 90 curing days. In an experimental study to assess the potential of alkali-silica reaction in alkali-activated slags, Fernández-Jiménez and Puertas [16] demonstrated that AA binders based on slags presented lower expansion rates in comparison to OPC mortar subjected to similar conditions.

The combination of blast furnace slag with other aluminosilicate materials has also been extensively reported in the production of alkali-activated binders [17–18]. In these cases, the main objective has been to explore the good properties of each precursor. This strategy is a new way to produce sustainable concrete that not only facilitates the reduction of CO_2 emissions, but also reuses different types of by-products [19].

There are many examples of these types of study. Deb et al. [17] explored the evolution of the workability and strength properties of GGBS and fly ash blends. Akçaözoğlu and Ulu [20] conducted experiments in which polyethylene terephthalate (PET) granules were used as aggregates in alkali-activated GGBS/metakaolin blended systems. Other authors such as Islam et al. [18] have also developed binders by the alkaline activation of palm oil fuel ash, GGBS and fly ash blends. These were activated with sodium silicate and sodium hydroxide solutions and cured at 65 ºC the first 24 hours and at room temperature for 7, 14 and 28 days.

The chemical composition of the sewage sludge ash – which is rich in alumina and silica – make it a good candidate for the production of alkali-activated binders. The alkaline activation of SSA has also been successfully proven by Yamaguchi and Ikeda [21] where fly ash/SSA blends were activated with sodium silicate and NaOH solutions. However, high curing temperatures (80 ºC) were required to activate the process, only one mix proportion was used for the alkaline activator, and no data on the compressive strength of the system were reported. Thus, further research on the influence of other types of alkaline activators (NaOH), concentration of the activating solution and curing conditions (e.g. room temperature) must be conducted to understand the influence of these type of ashes on the microstructure and mechanical properties of the newly developed binder.

Hence, the work reported in this paper aims to understand the influence of sewage sludge ash (SSA) and sodium concentration in the mechanical strength and microstructure development of alkali-activated GGBS-based binders cured at room temperature.

2. Experimental procedure
2.1. Equipment

Compressive strength was tested using a universal test machine from EMIC with a 200 ton load limit. The microstructure of raw materials and alkali-activated pastes were assessed using different instrumental techniques: X-ray fluorescence spectroscopy (FRX, Philips Magix Pro); Laser diffraction granulometry (Mastersizer 2000, Malvern Instruments); X-ray diffraction (Shimadzu X-Ray Diffractometer XRD-6000) from 5–55º with Cu Kα radiation at 30 kv and 40 mA; Fourier transformed infrared spectroscopy (FTIR) in transmittance mode, from 4000–400 cm^{-1} (NEXUS 670, Nicolet Instrument Corporation) and Scanning

electron microscopy (SEM, model EVOLS15 from Zeiss) using secondary electrons and 20 kV was used to examine the microstructure of both raw materials and fractured surfaces (covered with gold).

2.2. Materials

Alkali-activated binders were prepared using binary systems of ground granulated blast furnace slag (GGBS) and sewage sludge ash (SSA). GGBS was used as-received and it was supplied by Siderúrgica Ribas do Rio Pardo (Brazil). Sewage sludge was obtained from SeMAE (São José do Rio Preto – Brazil) and the ash was produced by burning the waste under controlled conditions (maximum temperature: 775 ºC), the resulting bottom ash was then ground using a ball mill for 50 minutes. Table 1 summarises the chemical composition of both the GGBS and the SSA determined using X-ray fluorescence analysis.

The SSA contained a higher amount of acid oxides $Al_2O_3+SiO_2 +Fe_2O_3$ than GGBS (70.27% and 45.03% for the SSA and GGBS respectively). Calcium was the most significant element found in GGBS. Loss on ignition (LOI) values for SSA was relatively low, suggesting that most of the organic matter was removed during the combustion process. Studies reported in the literature have shown that the chemical composition of sewage sludge ash can be highly varied, depending on the origin of wastewater, additives used on its treatment and the incineration system [8]. Nevertheless, for all cases, the main components of sewage sludge ashes are SiO_2, CaO, Al_2O_3, Fe_2O_3, MgO and P_2O_5 [4].

For this study, the SiO_2 content (38.28%) is close to the mean value reported by Cyr et al. [22] while Al_2O_3 content was found to be slightly higher. Significant amounts of phosphorus (7.28%; recorded as P_2O_5) were also found in the ash used in this study, this content is lower than the mean value reported in the literature [22]. The P_2O_5 percentage is close to that of the SSA used by Monzó et al. [11]. Similarly, the amount of CaO was lower in comparison to the mean values reported in the literature [8, 22], they were observed to vary within a wide range: 1.1–40.1% probably due to different treatments in the different wastewater plants.

Table 1. Chemical composition of raw materials (wt.%).

Oxide	GGBS	SSA	Other SSA [8, 22]		
			Mean	Min.	Max.
SiO_2	32.96	38.28	36.1	14.4	65.0
Al_2O_3	11.51	20.72	14.2	4.4	34.2
Fe_2O_3	0.56	11.27	9.2	2.1	30.0
CaO	43.54	5.51	14.8	1.1	40.1
P_2O_5		7.28	11.6	0.3	26.7
MgO	7.32	1.91	2.4	0.02	23.4
Na_2O	0.35	0.70	0.9	0.01	6.8
MnO	0.39	0.05	0.3	0.03	0.9
TiO_2	0.50	3.73	1.1	0.3	1.9
SO_3	1.89	4.18	2.8	0.01	12.4
K_2O	0.41	0.71	1.3	0.1	3.1
Other	0.47	2.24			
LOI	0.10	3.41	6.1	0.2	41.8

The mineralogy of SSA and GGBS was determined by X-ray powder diffraction (Figure 1). As expected from previous studies [23–24], amorphous phases characterised by the deviation of baseline in the 17–37º 2θ range were observed for GGBS. In the same way, some peaks identified as Quartz (SiO_2, PDF #781253) and calcite ($CaCO_3$, PDF #721651) were found as minor crystalline phases in the GGBS.
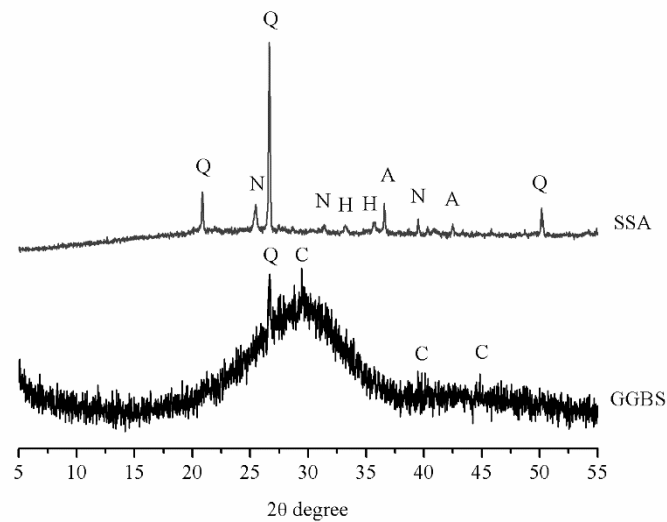
Figure 1. XRD patterns for GGBS and SSA. Keys: Q – quartz (SiO_2), C – calcite ($CaCO_3$), N – anhydrite ($CaSO_4$), H – hematite (Fe_2O_3) and A – albite ($NaAlSi_3O_8$).

In the XRD pattern for SSA, there was a slight baseline deviation in the 15–35º 2θ range, indicating the presence of amorphous phases. The presence of high quantities of crystalline compounds makes it difficult to distinguish the amorphous phase in SSA. In agreement with a review by Cyr et al. [22], the main crystalline compounds identified in the SSA analysed in this study were quartz and anhydrite ($CaSO_4$, PDF #72503). Minor crystalline phases were also found: albite ($NaAlSi_3O_8$, PDF#191184) and hematite ($Fe2O_3$, PDF #791741). Albite is not a compound commonly present in SSA; however its occurrence is reported in some studies [25]. Although the calcium phosphate known as whitlockite (β-$Ca_3(PO_4)_2$ or $Ca_7Mg_2P_6O_{24}$) has previously been identified in the literature [1, 22], no significant presence of this mineral was detected in this study. Similarly, calcite could not be clearly distinguished in the XRD results.

The particle size distribution of GGBS and ground SSA was determined using a laser diffraction technique under water suspension. The slag had a mean particle diameter of 27.50 μm, d (0.1) = 4.21 μm, d (0.5) = 21.42 μm and d (0.9) = 58.56 μm. In the case of SSA, the mean particle diameter was 20.27 μm, d (0.1) = 1.58 μm, d (0.5) = 11.77 μm and d (0.9) = 52.45 μm. Thus, SSA was finer than GGBS.

According to the SEM images (Figure 2), both materials presented a wide particle size distribution, with the slag particles being sharper and denser than the SSA. SSA is expected to present higher water absorption values than GGBS. This is due to its lower density, the larger amount of fine particles and the rough particle surfaces.
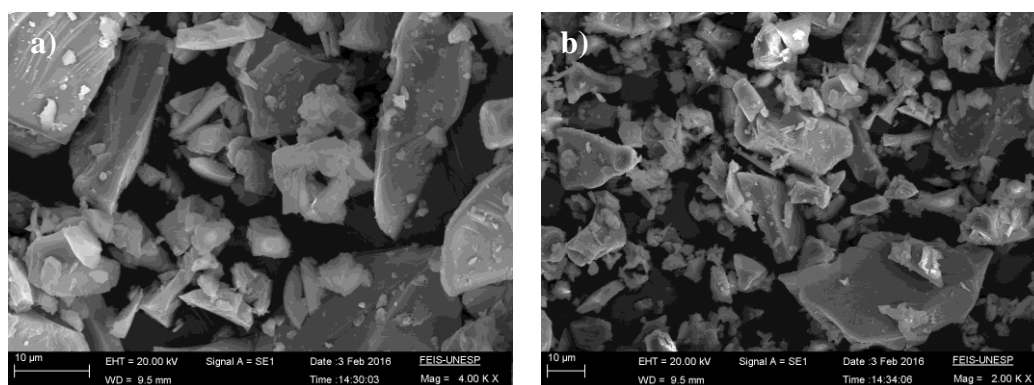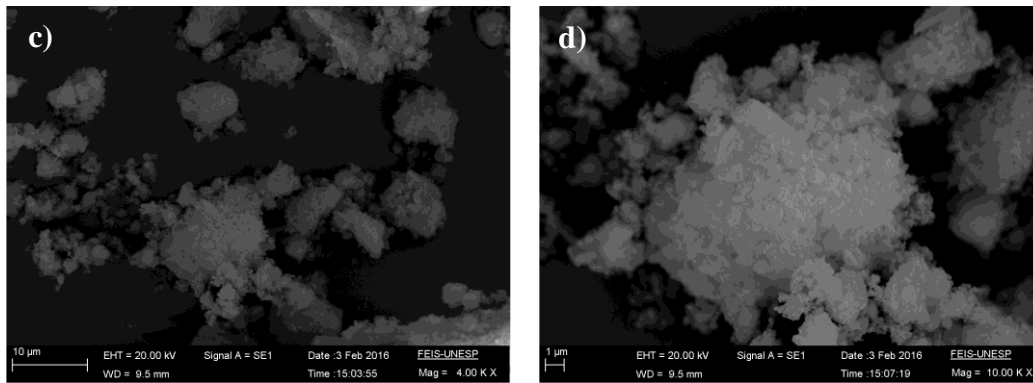
Figure 2. SEM images of raw materials: GGBS (a and b); ground SSA (c and d).

2.3. Preparation of pastes and mortars

Different percentages of SSA (0–30 wt.%) were used in substitution of GGBS. The alkaline activating solutions were prepared by mixing sodium hydroxide pellets (98% purity, Dinâmica Química Contenporânea, Brazil) and water. Sodium concentrations ranged from 6–10 mol.kg^{-1}. The water to binder ratio (w/b) used was 0.45, the binder being the sum of GGBS and SSA.

The appropriate amounts of GGBS and SSA were dry mixed until homogeneous blends were obtained. Pastes were manually prepared by mixing the blended powder with the required amount of alkaline solution for four minutes and stored at room temperature until the testing age.

A binder (GGBS+SSA) to sand ratio of 1:2.5 was used for all the prepared mortars. The mixing rate was 124 rpm: during the first 30 seconds the alkaline solution was homogenized; during the following 60 seconds, solid powder was gradually added; sand is then added in the mixture during the next 60 seconds; finally the fresh mortar was mixed for an additional 120 seconds. Mortars were compacted in cylindrical moulds (50 x 100 mm) using a vibration table and specimens were cured at room temperature (25 ºC, RH 96%) for 7, 28 and 90 days. For each curing time, five mortar specimens were mechanically tested. The parameters involved in the mixes for this study are summarised in Table 2.

Table 2. Dosages and curing conditions of pastes and mortars.

GGBS wt.%	SSA wt.%	w/b	$[Na^+]$ $Mol \cdot kg^{-1}$	Sand/binder	Curing conditions
100	0				
90	10		6		7, 28 and 90 days
80	20	0.45	8	2.5 :1	25 °C
70	30		10		

3. Results and discussion

3.1. Mechanical strength

Compressive strength values for mortars are summarised in Table 3. In general, all alkali-activated mortars displayed compressive strength in the range 17–25 MPa, independently of the percentage of SSA or the NaOH concentration. The best compressive strength value was obtained for mortar cured for 90 days with 6 mol.kg^{-1} NaOH and with 20% SSA (31.1 MPa).

Table 3. Compressive strength values for mortars (MPa).

		Compressive Strength (MPa)			
Curing time (days)	**NaOH (mol.kg^{-1})**	0%	10%	20%	30%
	6	17.1	17.6	16.2	11.5
7	8	13.8	15.9	15.1	17.1
	10	15.1	18.0	15.9	12.4
	6	24.6	20.8	30.8	23.6
28	8	19.6	21.0	22.2	21.2
	10	17.8	18.4	17.7	11.4
	6	24.2	25.4	31.1	26.0
90	8	20.9	22.6	23.0	21.4
	10	20.0	21.3	20.0	20.1

Figure 3 depicts the non-linear fitting surface of the compressive strength of alkali-activated mortars based on GGBS/SSA for 28 and 90 days of curing. A clear trend can be observed for this system: mortars

activated with 6 mol.kg^{-1} NaOH displayed higher compressive strengths than those obtained by using other activating solutions. This was true for all curing times. The use of SSA in the 10–20 wt.% range can be considered the optimum percentage for replacement.
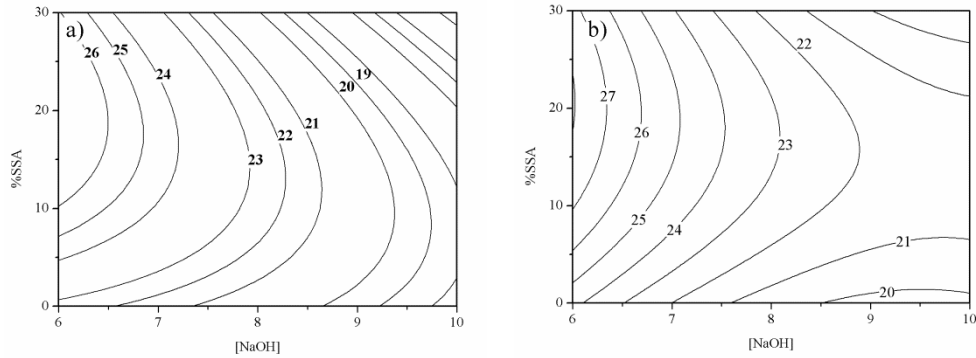

Figure 3. Non-linear fitting surface of compressive strength for alkali-activated GGBS/SSA: a) 28 curing days; b) 90 curing days.

3.2. X-ray diffraction (XRD)

Figure 4 shows XRD patterns for precursors (GGBS and SSA) and for selected alkali-activated pastes (0 wt.% SSA 6 mol.kg^{-1}, 20 wt.% SSA 6 mol.kg^{-1}, 20 wt.% SSA 8 mol.kg^{-1} and 20 wt.% SSA 10 mol.kg^{-1}). The crystalline phases present in raw materials (quartz, albite, hematite and calcite) did not react in the presence of the alkaline activating solution. The corresponding XRD peaks are observed in the XRD diffractogram for alkali-activated pastes. Additionally, the peaks relating to anhydrite were not detected in the alkali-activated pastes indicating that anhydrite is dissolved by the alkaline solution.

By comparing the XRD patterns of raw materials and alkali-activated pastes, the appearance of some baseline deviation in the diffractogram of alkali-activated pastes was observed. In a specific study related to the structural characterization of C-S-H and C-A-S-H using Rietveld analyses, Renaudin et al. [26] showed that the presence of the broad bands centred around 2θ degree of 7°, 16°, 29°, 32 and 50° were associated with the formation of amorphous phases such as C-S-H gel and C-A-S-H gel. Hence, the baseline deviation observed in the alkali-activated pastes can be attributed to the presence of calcium silicate hydrates (C-S-H), the major binding phases formed in the alkaline activation of GGBS. [24,27,28].

For pastes with 20 wt.% of SSA, it was observed that an increase of the NaOH concentration contributes to an increase of amorphous phase content.
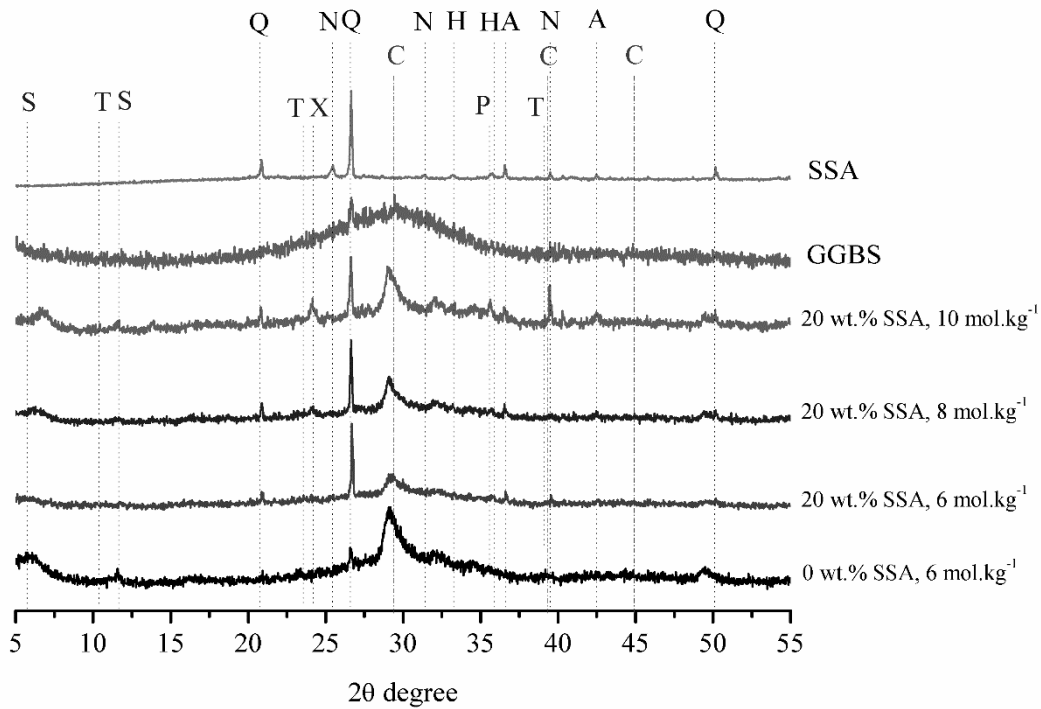

Figure 4. XRD patterns for raw materials and some alkali-activated pastes cured at 25 °C for 28 days. Key: Q – quartz, H – hematite, N – anhydrite, A – albite, C – calcite, S – stratlingite, T – hydrotalcite, X – hydrosodalite, and P – pirssonite.

Some crystalline phases were detected in the XRD pattern of the alkali-activated pastes. Pirssonite $(Na_2Ca(CO_3)_2.2H_2O$, PDF#220476) is a sodium carbonate compound formed due the reaction of sodium hydroxide with atmospheric CO_2 while in the presence of calcium. This crystalline phase was detected in the samples activated with the highest NaOH concentration solution (10 mol.kg^{-1} of NaOH), indicating an excess of sodium hydroxide in the mixture. Another carbonate-type formed during the alkaline activation of slags was hydrotalcite $(Mg_6Al_2CO_3(OH)_{16}.4H_2O$ PDF#140191). According to Wang and Scrivener [24], hydrotalcite is a typical hydrated product containing Mg and Al formed in the alkaline activation of GGBS. The mechanism formation of hydrotalcite is so difficult to discuss without knowing the exact form in which the Mg and Al exist [29]. In this study, hydrotalcite was mainly detected with pastes activated with 6 mol.kg^{-1} of NaOH, as reported by Wang [29].

The other crystalline phases are zeolite-types; these are commonly formed during the alkali-activated reaction. Hydrosodalite ($Na_6[AlSiO_4]6 \cdot (H_2O)_4$ PDF#42216), a zeolite-type, was detected mainly in pastes activated with high NaOH concentrations. This is most likely due to the reduction in the ratio of Ca^{+2}/Na^+, this favours the formation Na-zeolites in the alkaline activation of slags. According to Provis and van Deventer [30] small quantities of zeolites promote a mechanical strength gain for alkali-activated binders. Lastly, stratlingite ($2CaO.SiO_2.Al_2O_3.8H_2O$ PDF#290285) was also detected. This calcium silicoaluminate hydrate was also reported in the mineralogical analysis of GGBS binders.

3.3. Infrared spectroscopy

FTIR spectra of pastes with 20 wt.% of SSA, activated with 6–10 mol.kg^{-1} of NaOH solutions and cured at 25 ºC for 28 days have been plotted in Figure 5. Additionally, FTIR spectra for the raw materials SSA and GGBS have been included for comparison (Figure 5). Since there were no significant changes within the 4000–2000 cm^{-1} region, data has been plotted from 400–2000 cm^{-1}. A broad band around 3440 cm^{-1} was observed for all samples, this can be linked to another band arising at 1600 cm^{-1}. These bands are attributed to stretching and deformation vibrations of O-H groups [31].
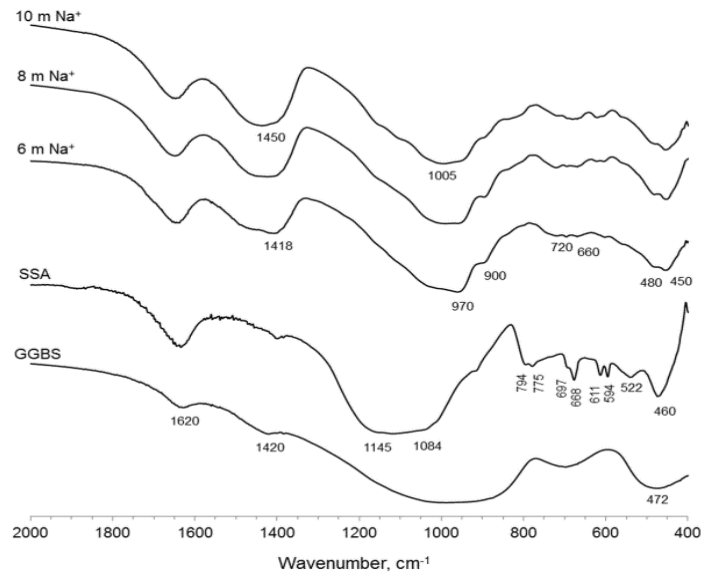

Figure 5. FTIR spectra for alkali-activated pastes containing 20 wt.% of SSA cured for 28 days.

For the SSA sample, the presence of quartz as main crystalline compound was corroborated using FTIR by the bands located at 1145, 1084, double band at 796–778, 697, 668, 522 and 460 cm^{-1} [32]. The GGBS spectrum presents a broad band at 1050–850 cm^{-1} related to the asymmetric stretching vibrations of the Si-O tetrahedral, a band centred at 472 cm^{-1} which corresponds to the deformation vibration (O-Si-O) and a band arising between 800–600 cm^{-1} that is attributed to the asymmetric stretching vibrations of Al-O bonds [23]. The band at 1420 cm^{-1} is attributed to stretching vibrations of CO_3^{-2} in carbonates [33–35]. It confirms the partial carbonation of the GGBS previously observed by XRD.

For alkali-activated pastes cured at room temperature for 28 days, a shift of bands to lower energy (compared to the raw materials) can be observed, indicating that the raw materials have reacted in the high alkaline media and that new binding structures, such as C-A-S-H gel or (N,C)-A-S-H gel, have been formed. No significant differences were found among pastes activated with 6–10 mol.kg^{-1} NaOH solutions.

A band centred at 960 cm^{-1} can be observed for all alkali-activated pastes, this is related to the asymmetric stretching vibrations of Si-O-T (T = Al, Si) bonds. This band is associated with the formation of hydrated products such as (N,C)-A-S-H gel [36]. As identified by Garcia-Lodeiro et al. [36], the displacement of sodium by calcium in the (N,C)–A–S–H gels does not imply relevant changes in the position of the bands, but the variation in its shape is a possible sign of the precipitation of new phases that are not typical components of C–S–H gels. In this sense, the hump observed at 815 cm^{-1} is characteristic of Si–O (C–S–H) stretching vibrations, while that arising at 670 cm^{-1} provides information on the structural order of C–S–H gel [31].

According to Juenger et al. [37], (N,C)-A-S-H gel is a highly cross-linked structure that usually produces zeolite-types as secondary reaction product which can be detected by FTIR. The zeolites can be detected by FTIR due the presence of bands located at 720 and 660 cm^{-1} [38]. In this study, these bands are enhanced for alkali-activated pastes activated with increased NaOH concentrations. These results are in agreement with the XRD analyses where the presence of hydrosodalite was detected within pastes activated with high NaOH concentration.
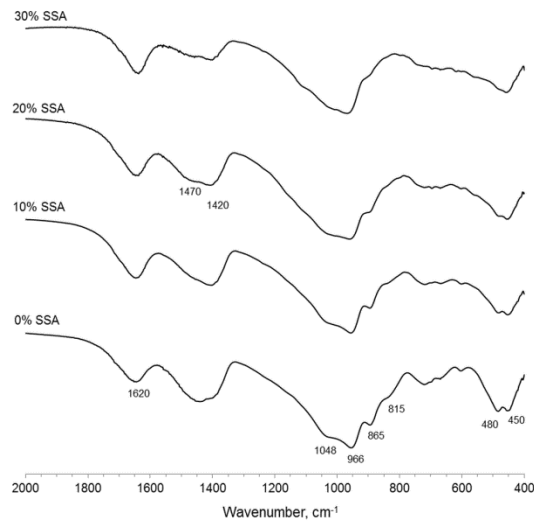
Figure 6. FTIR spectra for GGBS/SSA blends (0, 10, 20 and 30% of SSA) alkali-activated with 6 mol.kg^{-1} NaOH solutions, cured at 25 °C for 28 days.

Figure 6 shows the FTIR spectra for GGBS/SSA blends activated with 6 mol.kg^{-1} and cured at 25°C for 28 days. Although samples containing the highest SSA amounts (20 and 30 wt.%) and activated with the lowest sodium concentrations (6 mol.kg^{-1}) displayed a slight signal in the region corresponding to zeolitic products, the low alkali concentration observed in these signals cannot be clearly distinguished by FTIR. Signals typical of C–O stretching vibrations in carbonates appear in the range 1400–1600 cm^{-1} [34–35] and, whereas the lower wavenumber 1420 cm^{-1} is attributed to calcite-type bands, those appearing at 1470 cm^{-1} are assigned to other carbonate species such as pirssonite ($Na_2Ca(CO_3)_2.2H_2O$) and hydrotalcite ($Mg_6Al_2CO_3(OH)_{16}.4H_2O$) [39].

3.4. Scanning electron microscopy (SEM)

SEM micrographs of GGBS alkali-activated paste with 6–10 mol.kg^{-1} are shown in Figure 7. A typical compact microstructure [40] can be observed for alkali-activated pastes obtained by reaction between BFS and NaOH, in which compact C-A-S-H gel is the most important compound appearing as a gel-coating. This gel can be identified surrounding some unreacted slag particles. Additionally, some footprints from unreacted BFS particles were identified and were removed during the fracture. In some zones, small concentrations of a honeycomb-like C-A-S-H gel were also observed [41].
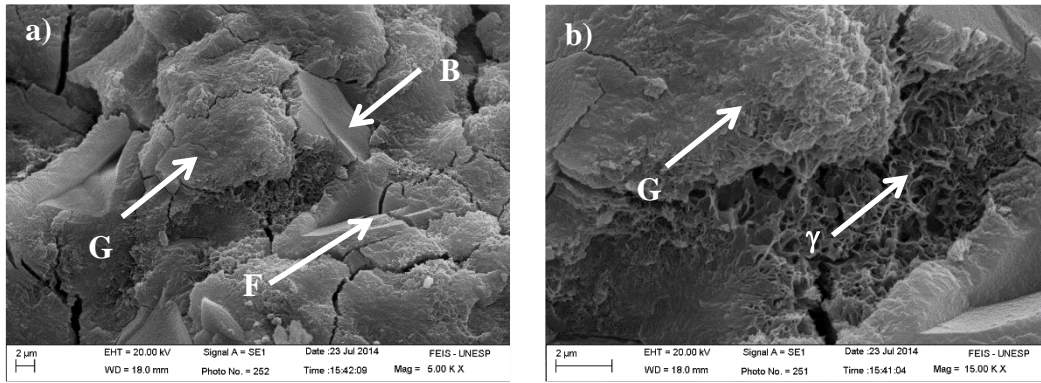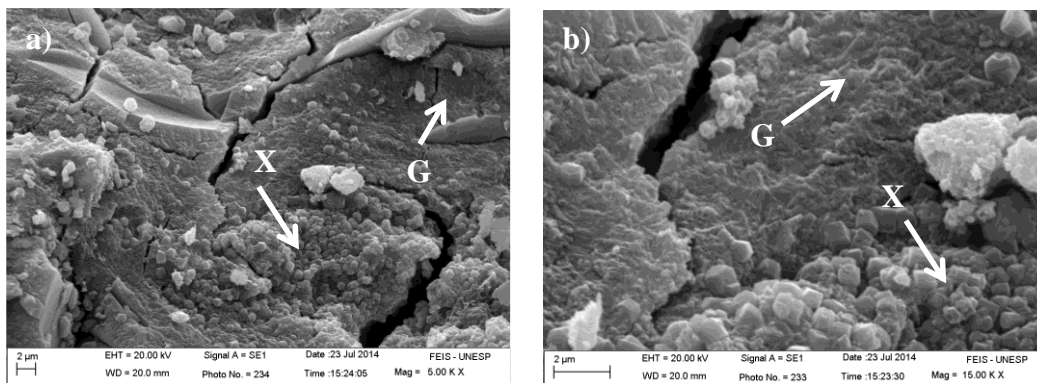
Figure 7. Scanning electron microscope images of GGBS (0 wt.% SSA) alkali-activated with 6 mol.kg^{-1} NaOH solution, cured at 25 ºC for 28 days: a) general view; b) detail of marked zone in a). [Key: compact C-A-S-H gel (G), honeycomb-like C-A-S-H gel (γ); unreacted BFS particle (B); footprint of unreacted BFS particle (F)].

In Figure 8, some zones in the 20 wt.% SSA paste are displayed. Large amounts of compact C-A-S-H gel was observed (Figure 8a and 8b) together with some small crystalline phases. Additionally, some honeycomb-like structure gel (Figure 8c) appears in low density zones. In these zones, small platelet-like particles (less than 2 µm length) were dispersed on the gel; these were most likely hydrotalcite crystals (Figure 8d). Crystalline phases dispersed on the compact gel (Figure 8e) were identified as hydrosodalite crystals [42]. In the magnification micrograph (Figure 8f), it can be seen that these crystals had a diameter less than 1 µm. Additionally, a quartz particle was observed, surrounded by these crystals: this particle did not react due to the crystallinity found in this type of silica, and it was present here because the SSA contained a significant amount of this mineral (see XRD pattern of SSA, Figure 1).
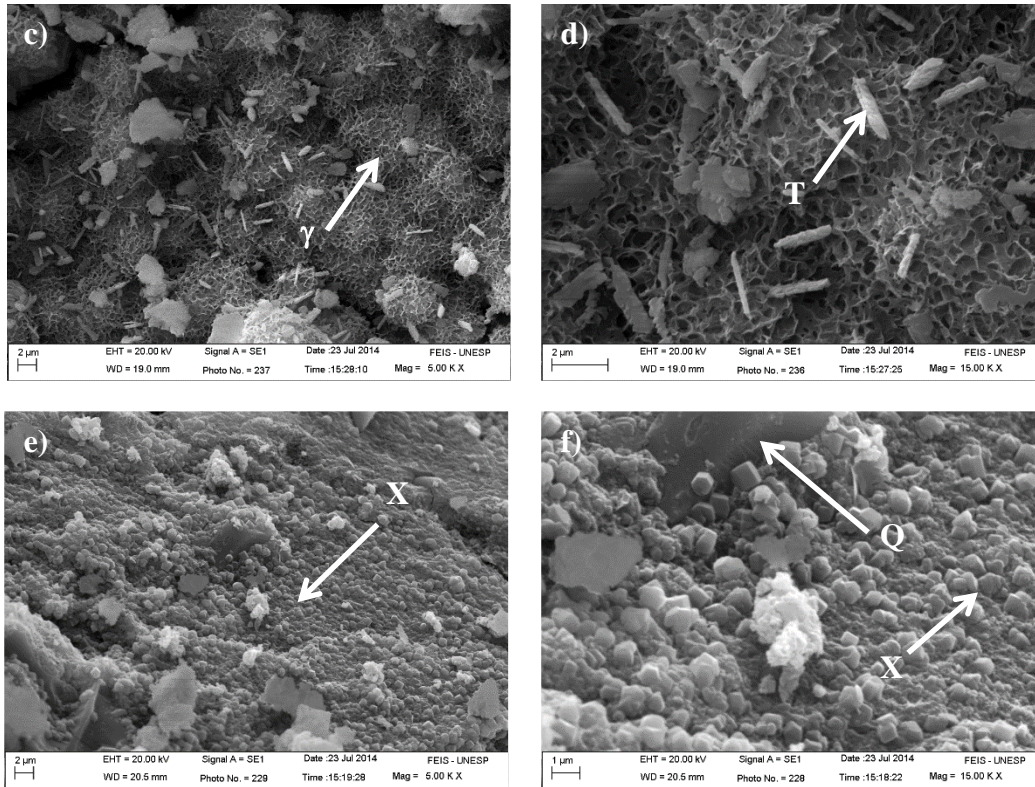
Figure 8. Scanning electron microscope images of GGBS/SSA blend (20 wt.% SSA), alkali-activated with 6 mol.kg^{-1} NaOH solution, cured at 25 ºC for 28 days: a) general view; b) detail of marked zone in a); c) zone with hydrosodalite crystals; d) detail for marked zone in c). [Key: compact C-A-S-H gel (G); honeycomb-like C-A-S-H gel (γ); hydrotalcite particles (T); hydrosodalite particles (X); quartz particle (Q)].

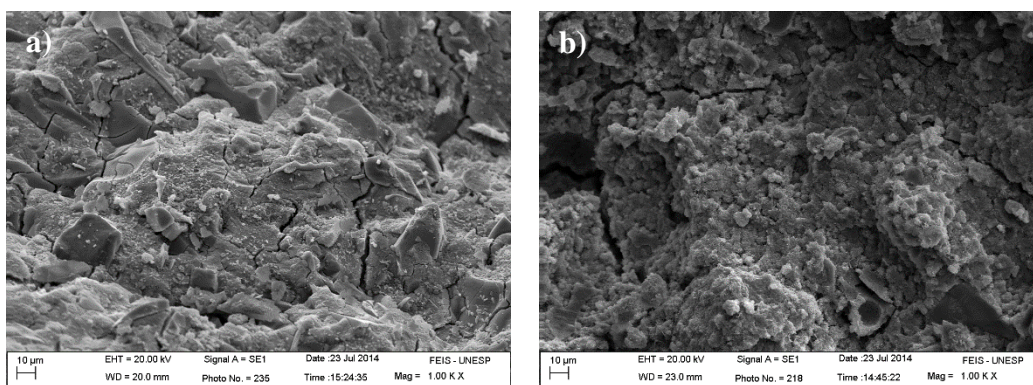Figure 9. Comparison between GGBF/SSA activated pastes (20 wt.% SSA): a) 6 mol.kg^{-1} NaOH solution; b) 10 mol.kg^{-1} NaOH solution.

Figure 9 displays a comparison between micrographs taken at x1000 magnification for pastes activated with 6 mol.kg^{-1} and 10 mol.kg^{-1} NaOH. It can be observed that an increase in the concentration of the alkali significantly altered the texture and porosity of the matrix. For the highest sodium concentration, the matrix developed higher porosity and less compact gel was observed. This result agrees with the mechanical behaviour of the corresponding mortars: at this curing age; compressive strength for mortar activated with 6 mol.kg^{-1} solution reached twice the strength of 10 mol.kg^{-1} activated mortars.
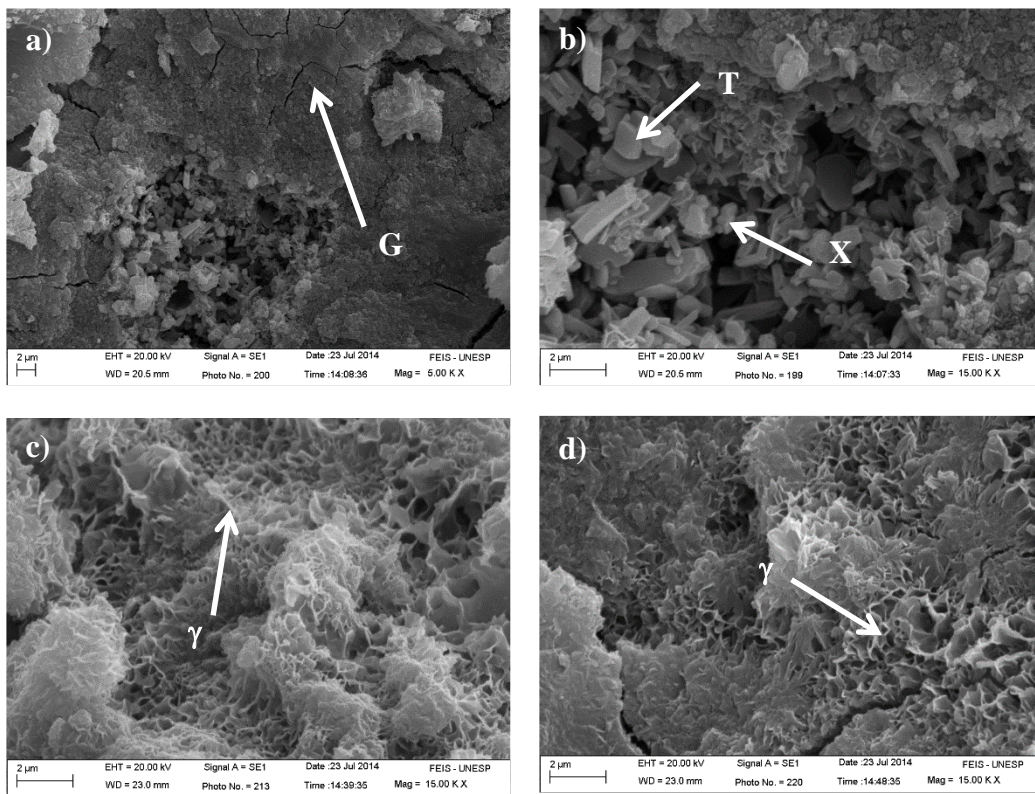

Figure 10. Scanning electron microscope images of GGBS/SSA blend (20 wt.% SSA), alkali-activated with: 8 mol.kg^{-1} NaOH solution (a and b); 10 mol.kg^{-1} NaOH solution (c and d). These were cured at 25 ºC for 28 days. [Key: compact C-A-S-H gel (G); honeycomb-like C-A-S-H gel (γ) ; hydrosodalite particles (X); hydrotalcite particles (T)].

SEM micrographs for pastes activated with 8 mol.kg^{-1} and 10 mol.kg^{-1} NaOH solutions are depicted in Figure 10. For paste activated with 8 mol.kg^{-1} NaOH, the presence of gel C-A-S-H can be seen (Figure 10a) mixed with other hydration products (probably hydrotalcite and hydrosodalite; Figure 10b). In Figures 10c and 10d, the honeycomb-type gel is observed for samples activated with 10 mol.kg^{-1} NaOH

solution. This gel, similar to that found for 6 mol.kg^{-1} activated paste (Figure 8b) displayed high porosity, with a pore size of less than 0.3 µm.

Comparing the microstructure of GGBS/SSA pastes (20 wt.% SSA) activated with 6 mol.kg^{-1} (Figure 8b and 8f) to pastes activated with 8 mol.kg^{-1} (Figure 10b, 10c and 10d), it can be noticed that the first one (6 mol.kg^{-1}) present a more denser and compacted microstructure than the second (8 mol.kg^{-1}). This fact certainly contributes to the compressive strength results of mortars activated with 6 mol.kg^{-1} that presented increased values when compared to the others alkaline activating solutions.

4. Conclusion

An alternative cementitious material has been developed at room temperature by the alkaline activation of ground granulated blast furnace slag and sewage sludge ash blends (GGBS/SSA). According to the results of this study, the following conclusions can be made:

- No significant reduction of the mechanical properties of alkali-activated GGBS mortars was observed at short curing ages when replacing up to 30 wt.% of GGBS with SSA.
- A significant contribution of the SSA to the mechanical properties of the GGBS mortars was observed after 28 curing days at room temperature, which allowed us to achieve up to 31 MPa under compression.
- Best compressive strength results were obtained in mortars blended with 20 wt.% SSA and activated with the lowest concentration NaOH solution (6 mol·kg^{-1}).
- The main reaction product was a cementitious gel, which was essentially of C-A-S-H type: compact gel was observed during the main cementing phase for 6 mol.kg^{-1} NaOH activated systems, and more porous gel was produced in systems activated with higher NaOH concentration solutions (8 and 10 mol.kg^{-1}).
- The mechanical properties of the developed mortars make them promising candidates to be used in construction applications. These have great environmental advantages over conventional alkali-activated binders because only NaOH solutions were used (no sodium silicate was required) and no additional energy was required to activate the process (e.g. thermal curing).

5. Acknowledgements

6. References

[1] Cheeseman, C.R., Virdi, G.S.: Properties and microstructure of lightweight aggregate produced from sintered sewage sludge ash. Resources, Conservation and Recycling. 45(1), 18–30 (2005)

[2] Pedrosa, M.M., Vieira, G.E.G., Sousa, J.F., Pickler, A.C., Leal, E.R.M., Milhomen, C.C.: Produção e tratamento de lodo de esgoto – uma revisão. Revista Liberato. 11(16), 149–160 (2010)

[3] Baeza-Brotons, F., Garces, P., Paya, P., Saval, J.M.: Portland cement systems with addition of sewage sludge ash. Application in concretes for the manufacture of blocks. Journal of Cleaner Production. 82, 112–124 (2014)

[4] Smol, M., Kulczycka, J., Henclik, A., Gorazda K., Wzorek, Z.: The possible use of sewage sludge ash (SSA) in the construction industry as a way towards a circular economy. Journal of Cleaner Production. 95, 45–54 (2015)

[5] Ministerio de Agricultura, Alimentación y Medio Ambiente. http://www.magrama.gob.es/es/calidad-y-evaluacion-ambiental/temas/prevencion-y-gestion-residuos/flujos/lodos-depuradora. Accessed 10 February 2016

[6] Donatello, S., Cheeseman, C.R.: Recycling and recovery routes for incinerated sewage sludge ash (ISSA): A review. Waste Management. 33(11), 2328–2340 (2013)

[7] Lynn, C.J., Dhir, R., Ghataora, G.S., West, R.P.: Sewage sludge ash characteristics and potential for use in concrete. Construction and Building Materials. 98, 767–779 (2015)

[8] Yusuf, R.O., Noor, Z.Z., Fadhil, M.D., Abba, A.H.: Use of sewage sludge ash (SSA) in the production of cement and concrete - a review. International Journal of Global Environmental Issues. 12(2/3/4), 214-228 (2012)

[9] Yang, J., Shi, Y., Yang, X., Liang, M,. Li, Y., Li, Y., Ye, N.: Durability of autoclaved construction materials of sewage sludge-cement-fly ash-furnace slag. Construction and Building Materials. 48, 398–405 (2013)

[10] Monzó, J., Payá, J., Borrachero, M.V., Peris-Mora, E.: Mechanical behavior of mortars containing sewage sludge ash (SSA) and Portland cements with different tricalcium aluminate content. Cement and Concrete Research. 29(1), 87–94 (1999)

[11] Monzó, J., Payá, J., Borrachero, M.V., Girbés, I.: Reuse of sewage sludge ashes (SSA) in cement mixtures: The effect of SSA on the workability of cement mortars. Waste Management. 23(4), 373–381 (2003)

[12] Tuan, B.L.A, Hwang, C.L., Lin, K.L., Chen, Y.Y., Young, M.P.: Development of lightweight aggregate from sewage sludge and waste glass powder for concrete. Construction and Building Materials. 47, 334–339 (2013)

[13] Lin, D.F., Chang, W.C., Yuan, C., Luo, H.L.: Production and characterization of glazed tiles containing incinerated sewage sludge. Waste Management. 28(3), 502–508 (2008)

[14] Reig, L. Tashima, M.M., Borrachero, M.V., Monzó, J., Cheeseman, C.R., Payá, J.: Properties and microstructure of alkali-activated red clay brick waste. Construction and Building Materials. 43, 98–106 (2013)

[15] Shi, C., Krivenko, P.V., Roy, D.: Alkali-activated cements and concretes. Taylor & Francis, London (2006)

[16] Fernández-Jimenéz, A., Puertas, F.: The alkali-silica reaction in alkali-activated granulated slag mortars with reactive aggregate. Cement and Concrete Research. 32, 1019–1024 (2002)

[17] Deb, P.S., Nath, P., Sarker, P.K.: The effects of ground granulated blast-furnace slag blending with fly ash and activator content on the workability and strength properties of geopolymer concrete cured at ambient temperature. Materials and Design. 62, 32–39 (2014)

[18] Islam, A., Alengaram, J.U., Jumaat, Z.M., Bashar, I.I.: The development of compressive strength of ground granulated blast furnace slag-palm oil fuel ash-fly ash based geopolymer mortar. Materials and Design. 56, 833–841 (2014)

[19] Duxson, P., Fernández-Jiménez, A., Provis, J.L., Lukey, G.C., Palomo, A., van Deventer, J.S.J.: Geopolymer technology: The current state of the art. Journal of Materials Science. 42(9), 2917–2933 (2007)

[20] Akçaözoğlu, S.: Recycling of waste PET granules as aggregate in alkali-activated blast furnace slag/metakaolin blends. Construction and Building Materials. 58, 31–37 (2014)

[21] Yamaguchi, N., Ikeda, K.: Preparation of geopolymeric materials from sewage sludge slag with special emphasis to the matrix compositions. Journal of the Ceramic Society of Japan. 118(1374), 107–112 (2010)

[22] Cyr, M., Coutand, M., Clastres, P.: Technological and environmental behavior of sewage sludge ash (SSA) in cement-based materials. Cement and Concrete Research. 37(8), 1278–1289 (2007)

[23] Torres-Carrasco, M., Rodríguez-Puertas, C., Alonso, M., Puertas, F.: Alkali activated slag cements using waste glass as alternative activators. Rheological behaviour. Cerámica y Vidrio. 54, 45–57 (2015)

[24] Wang, S.D., Scrivener, K.L.: Hydration products of alkali activated slag cement. Cement and Concrete Research. 25(3), 561–571 (1995)

[25] Wzorek, Z., Jodko, M., Gorazda, K., Rzepecki, T.: Extraction of phosphorus compounds from ashes from thermal processing of sewage sludge. Journal of Loss Prevention in the Process Industries. 19, 39–50 (2006)

[26] Renaudin, G., Russias, J., Leroux, F., Frizon, F., Cau-dit-Coumes, C.: Structural characterization of C-S-H and C-A-S-H samples-part I: long-range order investigated by Rietveld analyses. Journal of Solid State Chemistry. 182, 3312–3319 (2009)

[27] Li, C., Sun, H., Li, L.: A review: the comparison between alkali-activated slag (Si+Ca) and metakaolin (Si+Al) cements. Cement and Concrete Research. 40, 1341-1349 (2010)

[28] Puertas, F., Fernández-Jiménez, A., Blanco-Varela, M.T.: Pore solution in alkali-activated slag cement pastes. Relation to the composition and structure of calcium silicate hydrate. Cement and Concrete Research. 34, 139-148 (2004)

[29] Wang, S-D.: Alkaline activation of slag. PhD Thesis, Imperial College, University of London, 1995

[30] Provis, J.L., van Deventer, J.S.J.: Geopolymers, structure, processing, properties and industrial applications. Woodhead Publishing, New York (2009)

[31] García Lodeiro, I., Macphee, D.E., Palomo, A., Fernández-Jiménez, A.: Effect of alkalis on fresh C-S-H gels. FTIR analysis. Cement and Concrete Research. 39(3), 147–153 (2009)

[32] Criado, M., Fernández-Jiménez, A., Palomo, A.: Alkali activation of fly ash: Effect of the SiO_2/Na_2O ratio. Part I: FTIR study. Microporous and Mesoporous Materials. 106(1-3), 180–191 (2007)

[33] Pacewska, B., Nowacka, M., Wilińska, I., Kubissa, W., Antonovich V.: Studies on the influence of spent FCC catalyst on hydration of calcium aluminate cements at ambient temperature. Journal of Thermal Analysis and Calorimetry. 105(1), 129–140 (2011)

[34] Fernández-Carrasco, L., Torréns-Martín, D., Martínez-Ramírez, S.: Carbonation of ternary building cementing materials. Cement and Concrete Composites. 34(10), 1180–1186 (2012)

[35] Fernández-Carrasco, L., Vázquez, T.: Aplication de la espectroscopia infrarroja al estudio de cemento aluminoso. Materiales de Construcción. 46(241), 39–51 (1996)

[36] García-Lodeiro, I., Fernández-Jiménez, A., Palomo, A., Macphee, D.E.: Effect of calcium additions on N-A-S-H cementitious gels. Journal of the American Ceramic Society. 93(7), 1934–1940 (2010)

[37] Juenger, M.C.G., Winnefeld, F., Provis, J.L., Ideker, J.H.: Advances in alternative cementitious binders. Cement and Concrete Research. 41(12), 1232–1243 (2011)

[38] Granizo, M.L., Alonso, S., Branco-Varela, M.T., Palomo, A.: Alkaline activation of metakaolin : effect of calcium hydroxide in the products of reaction. Journal of the American Ceramic Society. 85(1), 225–231 (2002)

[39] Mozgawa, W., Deja, J.: Spectroscopic studies of alkaline activated slag geopolymers. Journal of Molecular Structure. 434–441 (2009)

[40] Palacios, M., Puertas, F.: Effect of shrinkage-reducing admixtures on the properties of alkali-activated slag mortars and pastes. Cement and Concrete Research. 37, 691–701 (2007)

[41] Rajaokarivony-Andriambololona, Z., Thomassin, J.H., Baillif, P., Touray, J.C.: Experimental hydration of two synthetic glassy blast furnace slags in water and alkaline solutions (NaOH and KOH 0.1 N) at 40 °C: structure, composition and origin of the hydrated layer. Journal of Materials Science. 25, 2399–2410 (1990)

[42] Liew, Y.M., Kamarudin, H., Mutafa al Bakri, A.M., Luqman, M., Khairul Nizar, I., Ruzaidi, C.M.: Processing and characterization of calcined kaolin cement powder. Construction and Building Materials. 30, 794–802 (2012)